



**Queensland University of Technology**  
Brisbane Australia

This is the author's version of a work that was submitted/accepted for publication in the following source:

Yang, Xilin, Mejias, Luis, & Bruggemann, Troy S. (2012) A 3D Collision Avoidance Strategy for UAVs in a Non-cooperative Environment. *Journal of Intelligent and Robotic Systems*. (In Press)

This file was downloaded from: <http://eprints.qut.edu.au/53391/>

**Notice:** *Changes introduced as a result of publishing processes such as copy-editing and formatting may not be reflected in this document. For a definitive version of this work, please refer to the published source:*

# A 3D Collision Avoidance Strategy for UAVs in a Non-cooperative Environment

Xilin Yang · Luis Mejias Alvarez · Troy Bruggemann

Received: date / Accepted: date

**Abstract** This paper presents a feasible 3D collision avoidance approach for fixed-wing unmanned aerial vehicles (UAVs). The proposed strategy aims to achieve the desired relative bearing in the horizontal plane and relative elevation in the vertical plane so that the host aircraft is able to avoid collision with the intruder aircraft in 3D. The host aircraft will follow a desired trajectory in the collision avoidance course and resume the pre-arranged trajectory after collision is avoided. The approaching stopping condition is determined for the host aircraft to trigger an evasion maneuver to avoid collision in terms of measured heading. A switching controller is designed to achieve the spatial collision avoidance strategy. Simulation results demonstrate that the proposed approach can effectively avoid spatial collision, making it suitable for integration into flight control systems of UAVs.

**Keywords** UAV · collision avoidance · switching control · PID control

## 1 Introduction

There has been an increasing number of UAV applications in the past few years due to their usefulness in a variety of situations following the success of several projects such as the *Global Hawk* [1], the *Predator* [2] and the *MQ-8B Firescout* [3]. UAVs have shown several advantages over manned aircraft such as low manufacturing and operational costs (depending on the UAV type), flexibility to accommodate different payloads and risk reduction of human lives (no pilot or crew), etc. These advantages have enabled UAVs as an indispensable platform for various flight missions ranging from intelligence, surveillance and reconnaissance to scientific investigations and battlefield loss assessment.

---

Xilin Yang, Luis Mejias Alvarez and Troy Bruggemann  
are with the Australian Research Center for Aerospace Automation  
and Queensland University of Technology, Brisbane, Australia.  
E-mail: {xilin.yang, luis.mejias, t.bruggemann}@qut.edu.au

本文提出了一种可行的固定翼无人机三维避碰方法。该策略的目标是在水平方向上获得所需的相对方位，在垂直方向上获得所需的相对高程，使宿主主机能够在三维空间中避免与入侵机的碰撞。在避碰过程中，主机将沿预定轨迹飞行，避碰后恢复预定轨迹。根据测得的航向，确定了主机规避避碰的接近停止条件。设计了一个切换控制器来实现空间避碰策略。仿真结果表明，该方法能有效避免空间碰撞，适合集成到无人机飞行控制系统中。

The risk of unexpected spatial aircraft collision increases when they share the same airspace with other vehicles. This is caused by the fact that pre-arranged flight trajectories for UAVs are designed with little consideration of potential encounter. Also, the problem of UAV sense-and-avoid has been identified as one of the most significant challenges facing the integration of UAVs in the national airspace [4,5].

The collision avoidance problem can be divided in two parts. The “sensing or detection” and the “avoidance” aspects, respectively. In this paper, we address the avoidance aspect of the problem by proposing an approach for 3D collision avoidance in a non-cooperative scenario. Here, “non-cooperative environment” refers to an environment where a host aircraft has no prior information on the flight trajectory of an intruder and cooperative communication between them is unavailable. Non-cooperative approaches are the most challenging aspects of the problem given the high uncertainty in the intruder state. We have previously investigated the problem from the passive sensor perspective [6–9].

Planar (2D) aircraft avoidance has been subject to extensive investigation in a considerable number of papers, and significant efforts have been made to deal with different problems in various scenarios [10–13]. Kochenderfer *et al.* [14] presented a decision-theoretic approach to developing a collision avoidance logic using probabilistic models of aircraft behavior. The proposed methodology is aimed at meeting the safety level with guarantee while lowering the false alert rate and simplifying the process of re-optimizing the logic in response to variations in airspeed and sensor capabilities. Saunders *et al.* [15] assumed a vision processing unit that provides object segmentation and a range estimate to nearby obstacles. The proposed nonlinear guidance law attempts to maneuver the UAV in such a way that the obstacle is moved to the edge of the camera field of view (FOV), maintaining the obstacle on the edge of FOV guarantees that trajectory of the UAV is not on the collision course with the obstacle. There are also some approaches which rely greatly on availability of a high-integrity GPS and a continuous data-link (e.g. automatic dependent surveillance broadcast (ADS-B) [16,17]).

Passive sensors also provide a means of identifying obstacles in different avoidance strategies [18–20]. Beyeler *et al.* [21] presented a novel control strategy for autonomous flight in the vicinity of obstacles with proximity of obstacles estimated using optic flow sensors. The proposed solution allows a UAV to fly and avoid obstacles using a simple sensor-to-actuator mapping by exploiting properties of translation-induced optic flow and the dynamics of flying platforms, thus eliminating the need for state information provided by GPS. Griffiths *et al.* [22] proposed an obstacle avoidance strategy based on the mapping information which utilizes laser range finder and optic flow sensors to detect the terrain. Flight tests were conducted to verify the feasibility of this method in real scenarios. A new passive approach to collision detection and avoidance with moving obstacles is proposed by Angelov *et al.* [23]. In this strategy, a maneuver based on the worst case scenario will be initiated

当UAV与其它飞机共用同一空域时，发生意外空间碰撞的风险会增加。这是由于预先设计的无人机飞行轨迹很少考虑潜在的相遇。此外，无人机感知与避障问题已被确定为无人机在国家空域集成所面临的最重大挑战之一[4,5]。

避障问题可分为两部分。分别是“感知或检测”以及“避免”方面。在这篇论文中，我们通过提出一种非合作情形下的三维避障方法来解决问题的避障方面。这里的非合作环境是指宿主主机对入侵者的飞行轨迹没有事先的信息，无法进行合作通信的环境。考虑到入侵者状态的高度不确定性，非协作方法是问题中最具挑战性的方面。我们之前已经从无源传感器的角度研究了这个问题[6-9]。

在相当多的文献中，平面(2D)飞机的避障已经受到了广泛的研究，在不同的场景下，人们已经做出了重大的努力来处理不同的问题[10-13]。Kochenderfer等人提出了一种利用飞机行为的概率模型来开发避障逻辑的决策理论方法。提出的方法旨在满足安全水平的保证，同时降低误报率和简化重新优化逻辑的过程，以响应变化的空速和传感器的能力。Saunders等人提出了一种视觉处理单元，该单元提供目标分割和对附近障碍物的距离估计。所提出的非线性制导律试图以使障碍物移动到摄像机视场(FOV)边缘的方式操纵无人机，将障碍物保持在FOV边缘可确保无人机的轨迹不在与障碍物的碰撞航迹上。还有一些方法在很大程度上依赖于高完整性GPS和连续数据链的可用性(如自动相关监视广播(ADS-B)[16,17])。

无源传感器还提供了一种识别不同躲避策略中障碍物的方法[18-20]。Beyeler *et al.* [21]提出了一种新的自主飞行控制策略，该策略利用光流传感器对障碍物附近的障碍物进行估计。该解决方案通过利用平移诱导的光流特性和飞行平台的动力学特性，允许无人机使用简单的传感器到执行器的映射来飞行和避免障碍，从而消除了对GPS提供的状态信息的需求。Griffiths等人提出了一种基于映射信息的避障策略，利用激光测距仪和光流传感器来检测地形。通过飞行试验验证了该方法在实际应用中的可行性。Angelov等人提出了一种新的被动避障方法，用于运动障碍物的碰撞检测和避障。在这种策略下，一旦检测到潜在的碰撞，将根据最坏的情况采取行动；然后，执行最优返回到预先计划的路线。

once a potential collision is detected. Afterwards, an optimal return to the pre-planned route will be executed.

The present research is part of efforts devoted to design a Sense and Avoid (SA) system for airspace collision avoidance. This system only relies on the detection of signals emanating from the targets themselves. Recently, motion detection using multiple cameras provides an attractive means of developing a SA system due to relatively low cost, size and power requirements for sensors. The basic paradigm of this technology is to use multiple cameras placed at different angles to create multiple views that, when combined, can allow for calculation of object vectors [24]. The challenge of motion detection is that a moving UAV makes it difficult to design a generic algorithm for different scenarios. Thus, various algorithms have been developed to deal with different scenarios to make distinction between the movement of the host aircraft and that of the intruder [25, 24, 26]. In practice, these algorithms cancel the movement of the UAV, including movement based on vehicle trajectory, as well for vibration from the UAV. Currently, there are only a few authors addressing spatial (3D) collision avoidance. Christodoulou *et al.* [27] formulated the confliction avoidance problem in three-dimension as a mixed-integer nonlinear programming problem, and the total flight time to avoid possible conflicts were obtained. In the present work, we aim to develop a 3D aircraft collision avoidance system based on measured heading information. During normal flight course, UAVs are commanded to achieve steady-state flight conditions for most of the flight duration. Therefore, it is reasonable to assume that both host aircraft and intruder are with constant velocity before the collision is detected. The relative bearing is also assumed to be measurable in the considered application. Cameras onboard the host aircraft are used to estimate the desired relative bearing and relative elevation with respect to the intruder aircraft during the approach process. The host aircraft resumes the pre-arranged route after collision avoidance. By completing these tasks, the intruder aircraft can be kept within the FOV of the camera. Moreover, a switching control system is designed to command the UAV to achieve collision avoidance during the encounter course.

目前的研究是致力于设计一个感知和避免 (SA) 系统的努力的一部分, 避免空域冲突。该系统只依赖于检测来自目标本身的信号。近年来, 由于传感器相对较低的成本、尺寸和功耗要求, 使用多摄像头进行运动检测成为一种很有吸引力的SA系统开发手段。该技术的基本范例是使用放置在不同角度的多个摄像头来创建多个视图, 当这些视图组合在一起时, 可以计算对象向量 [24]。运动检测的难点在于运动的无人机难以设计出适用于不同场景的通用算法。因此, 已经开发了各种算法来处理不同的场景, 以区分主机飞机的移动和入侵者的移动 [25, 24, 26]。在实践中, 这些算法消除了无人机的运动, 包括基于飞机轨迹的运动, 以及无人机的振动。目前, 解决空间 (3D) 避碰问题的作者较少。Christodoulou 等人将三维冲突避免问题转化为一个混合整数非线性规划问题, 得到了避免冲突的总飞行时间。在本工作中, 我们的目标是开发一个基于实测航向信息的三维飞机避碰系统。在正常飞行过程中, 无人机被要求在大部分飞行时间内保持稳定的飞行状态。因此, 可以合理地假设, 在检测到碰撞之前, 主机和入侵者的速度都是恒定的。在考虑的应用中, 相对方位角也被认为是可测量的。主飞机上的摄像头被用来在接近过程中估计所需的相对方位和相对高度。主机避碰后恢复预定航线。通过完成这些任务, 入侵者飞机可以保持在摄像机的视场 FOV (field of vision) 内。设计了一种切换控制系统, 实现了无人机在遭遇过程中的避碰控制。

The remainder of the paper is organized as follows: Section 2 describes collision avoidance in a 2D scenario. This is achieved by designing a planar spiral trajectory for the host aircraft. In Section 3, we extend the collision strategy to a 3D scenario where the host aircraft keeps the desired relative bearing with respect to the intruder aircraft and a relative elevation in the vertical direction. Design of the control system to implement the proposed collision strategy is given in Section 4. In Section 5, simulation results are given for typical 3D collision avoidance scenarios. Section 6 concludes this paper.

本文的其余部分组织如下: 第2节描述二维场景中的冲突避免。这是通过为主飞机设计一个平面螺旋轨迹来实现的。在第3节中, 我们将碰撞策略扩展到一个3D场景, 在该场景中, 主机保持所需的相对于入侵者飞机的相对方位和垂直方向的相对高度。第4节给出了为实现所提出的碰撞策略而设计的控制系统。第五部分给出了典型三维避碰场景的仿真结果。第六部分是本文的结论。

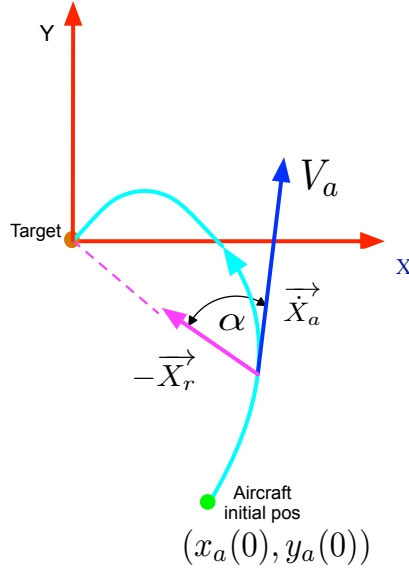


**Fig. 1** A UAV approaches a stationary target keeping a constant bearing  $\alpha$

## 2 Collision Avoidance of a Stationary Target

In this section, we begin analyzing the trajectory followed when an aircraft maneuvers to avoid a stationary target. The collision avoidance problem is investigated in the planar case. Let us define, a polar and a Cartesian coordinate frames with both origins located at the position of the stationary target, as shown in Fig. 1. The aircraft starts from initial position  $(x_a(0), y_a(0))$  with a constant speed of  $V_a$ . Any point on the maneuvering trajectory is described by  $(x_a, y_a)$  in Cartesian coordinates and  $(r, \theta)$  in polar coordinates. Here, aircraft heading is denoted by  $\theta$  which is the angle between  $x$ -axis and flight direction.

在这一节中，我们开始分析飞机在躲避固定目标时所遵循的轨迹。研究了平面情况下的避碰问题。我们定义，一个极坐标系和一个笛卡尔坐标系，它们的原点都位于静止目标的位置，如图1所示。飞机从初始位置  $(x_a(0), y_a(0))$  以一个恒定的速度  $V_a$  机动。机动轨迹上任意点描述  $(x_a, y_a)$  在笛卡尔坐标和极坐标  $(r, \theta)$ 。这里，飞机航向是用  $x$  轴和飞行方向之间的夹角  $\theta$  来表示的。

**Theorem 1** *The path of an aircraft flying at a constant velocity  $V_a$  with a constant relative bearing  $\alpha$  to a stationary target constructs an equiangular spiral trajectory.*

定理1：飞机以恒定的速度  $V_a$  且有不变的相对方位角  $\alpha$  飞向一个静止目标的路径构成了一条等角的螺旋轨迹。

**Proof:** This proof is excerpted from [28]. Cartesian coordinate of the aircraft can be related to its polar coordinates by the following expression,

$$x_a(t) = r(t) \cos \theta(t) \quad (1)$$

$$y_a(t) = r(t) \sin \theta(t). \quad (2)$$

Differentiating these equations leads to

$$\dot{x}_a = \dot{r} \cos \theta - r \dot{\theta} \sin \theta \quad (3)$$

$$\dot{y}_a = \dot{r} \sin \theta + r \dot{\theta} \cos \theta. \quad (4)$$

It is observed from Fig. 1 that the relative bearing is the angle between flight direction  $\dot{\mathbf{X}}_a$  and line-of-sight  $(-\mathbf{X}_r)$ . Here, relative range  $\mathbf{X}_r$  is described by the vector  $(x_a, y_a)$ . The constant bearing  $\alpha$  indicates

$$\frac{\dot{\mathbf{X}}_a \cdot (-\mathbf{X}_r)}{\|\dot{\mathbf{X}}_a\| \|(-\mathbf{X}_r)\|} = \cos \alpha, \quad (5)$$

which takes the explicit form of

$$\frac{-(x_a \dot{x}_a + y_a \dot{y}_a)}{\sqrt{x_a^2 + y_a^2} \sqrt{\dot{x}_a^2 + \dot{y}_a^2}} = \frac{-\dot{r}}{\sqrt{\dot{r}^2 + \dot{\theta}^2 r^2}} = \cos \alpha. \quad (6)$$

The assumption that the aircraft approaches with a constant velocity  $V_a$  gives

$$\sqrt{\dot{x}_a^2 + \dot{y}_a^2} = \sqrt{\dot{r}^2 + \dot{\theta}^2 r^2} = V_a. \quad (7)$$

Thus, Eq. (6) can be rearranged as

$$\dot{r} = -V_a \cos \alpha, \quad (8)$$

and the solution can be obtained with initial condition  $r(0) = r_0$

$$r(t) = -V_a t \cos \alpha + r_0. \quad (9)$$

Substituting Eq. (8) into Eq. (7) leads to a differential equation in terms of heading  $\theta$  which yields the solution described by

$$\theta(t) = \theta_0 - \ln\left(1 - \frac{V_a t}{r_0} \cos \alpha\right) \tan \alpha, \quad (10)$$

subject to the time constraint  $0 < t < r_0/(V_a \cos \alpha)$ .

The trajectory can also be expressed in terms of range and heading by replacing time  $t$  in Eq. (9) with Eq. (10),

$$r(\theta) = r_0 e^{(\theta_0 - \theta) \cot \alpha}. \quad (11)$$

This is the equation of equiangular motion. For any point on the trajectory, the intersection angle between the flight direction and line-of-sight is constant  $\alpha$ .

The following theorem gives the last time moment when the host aircraft should trigger an evasive maneuver. The time moment is only dependant on measurements of heading.

**Theorem 2** *Given minimum range  $r_{min}$  ( $r_{min}$  is the radius of the minimum allowable flight circle), the aircraft can keep a constant relative bearing  $\alpha$  during the encounter course until the time moment  $t^*$  given by*

$$t^* = \frac{r_0(1 - e^{(\theta_0 - \theta^*) \cot \alpha})}{V_a \cos \alpha}. \quad (12)$$

定理2：给定最小范围 $r_{min}$ （ $r_{min}$ 是最小允许飞行圆的半径），飞机可以在相遇过程中保持恒定的相对方位角 $\alpha$ ，直到由：

where the maximum allowable  $\theta^*$  is determined by

$$\theta^* = -\tan \ln \frac{r_{min}}{r_0} + \theta_0, \quad (13)$$

and

$$\theta^* > \theta_0 \text{ when } \alpha \in (0, \pi/2). \quad (14)$$

Proof: Given the minimum relative range  $r_{min}$ , the maximum allowable heading  $\theta^*$  can be obtained from Eq. (11), which takes the form of Eq. (13). Therefore, the last time moment to trigger evasion maneuver for collision avoidance can be obtained from Eq. (10), which is expressed as Eq. (12).

It is noticed from Eq. (12) that the evasion time  $t^*$  is related to the initial relative range  $r_0$ . In our case, the only available information is heading angle  $\theta$  and relative bearing  $\alpha$ , and we proceed to estimate  $r_0$  based on these information. We firstly collect sufficient measurements of  $\theta_i, i = 1, \dots, N$  where  $N$  indicates the number of samples. According to Eq. (11), relative range  $r_i$  at different sampling time is described by

$$r_i(\theta_i) = r_0 e^{(\theta_0 - \theta_i) \cot \alpha}, \quad i = 1, \dots, N, \quad (15)$$

which can be transformed into

$$\ln r_i = \ln r_0 + (\theta_0 - \theta_i) \cot \alpha, \quad i = 1, \dots, N \quad (16)$$

Introducing the following notation

$$x_i = \ln r_i, \quad i = 0, \dots, N \quad (17)$$

$$b_j = (\theta_0 - \theta_j) \cot \alpha, \quad j = 1, \dots, N, \quad (18)$$

converts Eq. (16) into a linear algebraic equation

$$AX = B, \quad (19)$$

where

$$A = \begin{bmatrix} -1 & 1 & & & \\ -1 & 0 & 1 & & \\ -1 & 0 & 0 & -1 & \\ \vdots & \vdots & \vdots & \vdots & \ddots \\ -1 & 0 & \dots & \dots & 1 \end{bmatrix} \in R^{N \times (N+1)}; \quad (20)$$

$$X = [x_0, x_1, \dots, x_N]^T \in R^{(N+1) \times 1}; \quad (21)$$

$$B = [b_1, \dots, b_N]^T \in R^{N \times 1}. \quad (22)$$

Since the number of unknowns is larger than that of equations, equation (19) is under-determined and the minimum norm solution can be obtained which satisfies  $\min \|AX - B\|_2$ . The solution takes the form of

$$\hat{X} = A^* B, \quad A^* = A^T (AA^T)^{-1}, \quad (23)$$



where  $A^*$  is pseudo-inverse of  $A$ . Once the solution  $\hat{X}$  is obtained, the initial relative range  $r_0$  can be obtained using the Eq. (17). Measurement noise is an inevitable factor affecting estimation performance of the algorithm in real applications. In the considered application, white noise is added to measurements of heading to check performance of the proposed algorithm, shown in Section 5.

### 3 Spatial Collision Avoidance of a Moving Intruder

We consider avoiding the spatial collision with a moving intruder under constant speed assumptions during the encounter course. The relative bearing  $\alpha_r$  and elevation  $\beta_r$  during the encounter course are described by

$$\alpha_r = \arctan \frac{y_a - y_t}{x_a - x_t}, \quad (24)$$

$$\beta_r = \arctan \frac{z_a - z_t}{x_a - x_t}, \quad (25)$$

where  $(x_a, y_a, z_a)$  are position coordinates of the host aircraft, and  $(x_t, y_t, z_t)$  are position coordinates of the intruder. The spatial encounter scenario assumes that the host aircraft and the intruder move with constant speeds towards each other and a potential collision will occur unless an avoidance maneuver is triggered. Here, the assumption that the intruder follows a straight flight with a constant velocity is reasonable since the encounter course does not persist for a long time and the intruder does not perform abrupt or aggressive maneuvers. When the host aircraft detects the intruder with the heading  $\theta_0$ , relative range  $r_0$  can be estimated using the method proposed in Section 2 based on measured heading collected up to the period of time when the encounter course occurs. Given the minimum allowable relative range, a switching controller is triggered to avoid the possible collisions and the aircraft is expected to maintain relative bearing  $\alpha_r$  in the horizontal plane and relative elevation  $\beta_r$  in the vertical plane. This is implemented by design of controllers in consideration of actuator capability. After collision avoidance is achieved, the host aircraft is commanded by the switching controller to resume the pre-arranged flight trajectory. For a stationary object, the requirement that the relative bearing is constant generates a spiral horizontal approaching trajectory. For a moving intruder, it will be seen that, owing to the movement of relative kinematics, the resultant horizontal trajectory tends to be spiral-like during the collision avoidance course due to the variations in the relative bearing.

The kinematic equations used to describe motion of the aircraft are

$$\dot{x}_a = V_a \cos \theta \cos \gamma, \quad (26)$$

$$\dot{y}_a = V_a \sin \theta \cos \gamma, \quad (27)$$

$$\dot{z}_a = V_a \sin \gamma. \quad (28)$$

我们考虑在恒定速度假设下，在遭遇过程中避免与移动入侵者的空间碰撞。在遭遇路线期间，相对方位角  $\alpha_r$  和海拔标高  $\beta_r$  由下式描述：



where  $(\dot{x}_a, \dot{y}_a, \dot{z}_a)$  are velocity components of the aircraft.  $\theta$  is heading angle and  $\gamma$  denotes flight path angle. The dynamic motion of velocity  $V_a$ , heading  $\theta$  and flight path angles  $\gamma$  can be described by [29]

$$\dot{V}_a = \frac{1}{m}[Y \sin \beta + (T \cos a - D) \cos \beta] - g \sin \gamma, \quad (29)$$

$$\begin{aligned} \dot{\theta} = & \frac{1}{mV_a \cos \gamma}[(L + T \sin a) \sin \sigma \\ & + Y \cos \sigma \cos \beta + (D - T \cos a) \cos \sigma \sin \beta], \end{aligned} \quad (30)$$

$$\begin{aligned} \dot{\gamma} = & \frac{1}{mV_a}[(L + T \sin a) \cos \sigma + (T \cos a - D) \\ & \cdot \sin \sigma \sin \beta - Y \sin \sigma \cos \beta] - \frac{1}{V_a}g \cos \gamma, \end{aligned} \quad (31)$$

where  $V_a$  is the aircraft velocity,  $m$  the mass of the aircraft,  $g$  the gravitational acceleration,  $a$  the angle of attack,  $\beta$  the sideslip angle,  $\gamma$  the flight-path angle,  $\sigma$  the bank angle (rotation about the velocity vector),  $L$  the lift force,  $D$  the drag force and  $T$  the thrust force.

The lift force  $L$  is described as

$$\begin{aligned} L = & \bar{q}S_w C_L \\ C_L = & C_{L0} + C_L^a a + C_L^{\delta_f} \delta_f + C_L^{\delta_e} \delta_e \\ & + \frac{c}{2V_a}(C_L^{\dot{a}} \dot{a} + C_L^q q) + C_L^M M. \end{aligned} \quad (32)$$

Here the dynamic pressure is  $\bar{q} = 0.5\rho V_a^2$  and  $\rho$  is the air density.  $S_w$  is the wing planform area. Explanations to aerodynamic coefficients  $C_{L0}$  and  $C_L^{(\cdot)}$  are given in [30].  $\delta_f$  and  $\delta_e$  are flap and elevator control command.  $q$  and  $M$  are pitching rate and pitching moment.

Thrust  $T$  is given by

$$T = \bar{q}S_D T_c \quad (33)$$

where  $S_D$  is the area of disc swept out by a propeller blade and  $T_c$  is the thrust coefficient.

The drag force  $D$  is expressed as

$$\begin{aligned} D = & \bar{q}S_w C_D \\ C_D = & C_{D0} + \frac{(C_L - C_{L0})^2}{\pi e AR} + C_D^{\delta_f} \delta_f + C_D^{\delta_a} \delta_a \\ & + C_D^{\delta_r} \delta_r + C_D^M M, \end{aligned} \quad (34)$$

and side force  $Y$  is

$$\begin{aligned} Y = & \bar{q}S_w C_Y \\ C_Y = & C_Y^\beta \beta + C_Y^{\delta_a} \delta_a + C_Y^{\delta_r} \delta_r + \frac{b}{2V_T}(C_Y^p p + C_Y^r r), \end{aligned} \quad (35)$$

Here,  $e$  is the efficiency factor and  $AR$  is the aspect ratio.  $\delta_a$  and  $\delta_r$  are aileron and rudder control command. Details for aerodynamic coefficients  $T_c$ ,  $C_D^{(\cdot)}$  and  $C_Y^{(\cdot)}$  can be found in [30].

To construct a realistic collision scenario, the host aircraft is commanded to move with steady-state flight conditions. This indicates the velocity, angle of attack and pitch angle are kept constant, and accelerations and angular rates are stabilized to zero. For the UAV model, throttle, elevator and aileron are properly actuated to achieve steady-state flight in consideration of structural limitations and servo dynamics constraints. The thrust force is controlled by choosing appropriate angular speed of engine. Due to the absence of flaps and rudders onboard the UAV, bank and yaw motion are controlled through commanding aileron actuators. The bank-to-turn (BTT) control mechanism is employed and two proportional-integral-derivative (PID) controllers are designed. The first one takes the desired yaw motion as input and stabilizes the yaw motion to the desired level. The yaw error is then input into the BTT PID controller and the command is converted to actuate the aileron to stabilize the bank motion in consideration of roll limit. The pitch and altitude are controlled by deflecting the elevator and a PID controller is designed for this purpose.

The symmetric flight conditions  $\beta = 0, Y = 0$  convert Eq. (29)-(31) into

$$\dot{V}_a = \frac{1}{m}((T \cos a - D) - g \sin \gamma), \quad (36)$$

$$\dot{\psi} = \frac{1}{mV_a \cos \gamma}(L + T \sin a) \sin \phi, \quad (37)$$

$$\dot{\gamma} = \frac{1}{mV_a}(L + T \sin a) \cos \phi - \frac{g \cos \gamma}{V_a}. \quad (38)$$

Here, we assume roll angle ( $\phi$ ) and bank angle ( $\sigma$ ) are approximately equal due to the small quantity of the angle of attack  $a$ . When steady-state flight is achieved, the host aircraft moves with an constant velocity and yawing angle. Also, the stabilized pitch  $\Theta$  and angle of attack  $a$  indicate that flight-path angle  $\gamma = \Theta - a$  is also constant.

#### 4 Design of the Switching Control System for Collision Avoidance

The control objective is to keep desired relative bearing  $\alpha$  and relative elevation  $\beta$  during the encounter course. To implement the proposed strategy, a switching control scheme consisting of a pre-arranged controller and a collision avoidance controller is designed, as shown in Fig. 2. For free flight conditions, the pre-arranged controller generates flight trajectories in consideration of operational and flight envelope requirements. Normally, routine control algorithms are programmed and saved on the flight computer and the most suitable one is chosen for the specific airspace environment. Such a controller aims to achieve steady-state flight without consideration of the potential conflict collision. During the encounter course, the collision avoidance controller

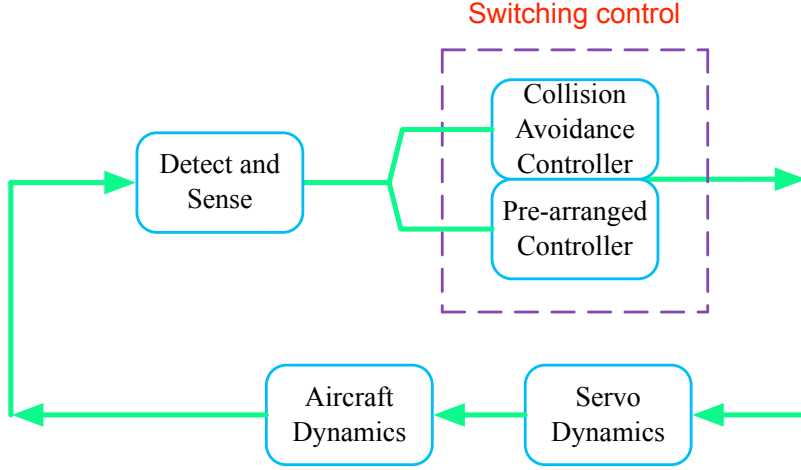


**Fig. 2** The switching control system for collision avoidance

is triggered once the potential collision is identified by the detect and sense system on the host aircraft. It arranges an evasive flight trajectory subject to the constraints that the relative bearing and elevation are desired values.

It is found that the desired bearing of the host aircraft should be tuned to generate an anticipative flight trajectory subject to operational constraints when the aircraft is at close vicinity of the intruder. Practically, it is infeasible for the aircraft to consistently follow the spiral trajectory after collision avoidance is completed. Thus, as the aircraft is out of the potential collision region, pre-arranged flight control can be resumed.

A switching controller is introduced to initiate the collision avoidance controller when potential collision is detected, which is triggered by the estimated relative range (relative range is estimated in the horizontal plane). Once the relative range reaches the threshold, collision avoidance controller is activated to generate aileron and elevator command, i.e.,

$$\psi_{cmd} = \begin{cases} k_p^\psi e_1 + k_i^\psi \int e_1 dt + k_d^\psi \frac{de_1}{dt} & t < t_1 \\ k_p^\psi e_2 + k_i^\psi \int e_2 dt + k_d^\psi \frac{de_2}{dt} & t_1 < t < t_2 \\ 0, & t > t_2 \end{cases}$$

where  $e_1 = \psi^d - \psi$ ,  $e_2 = \arctan \frac{y_a - y_t}{x_a - x_t} + \alpha_r^d - \psi$ . The term  $\arctan \frac{y_a - y_t}{x_a - x_t} + \alpha_r^d$  denotes the desired yaw of the host aircraft during the encounter course. The yaw command  $\psi_{cmd}$  is subject to constraints  $\psi_{min} \leq \psi_{cmd} \leq \psi_{max}$ , and it resumes to zero after the collision avoidance is completed.  $(x_a, y_a)$  are horizontal positions of the host aircraft, and  $(x_t, y_t)$  of the intruder.  $k_p^\psi$ ,  $k_i^\psi$  and  $k_d^\psi$  are proportional, integral and derivative gains of the PID controller. Zero yaw command indicates that current heading is the desired heading, and there is no need to drive the BTT to change the yawing. The host aircraft maintains the

current heading and travels in straight line. The time moment  $t_1$  triggers the collision avoidance controller which is determined by the threshold of the estimated relative range.  $t_2$  is the time moment to resume the straight-line flight after collision avoidance which is determined by the relative bearing angle  $\alpha_r$ . This is the time when the relative bearing angle is less than a prescribed angle. The prescribed angle is defined by the relative angle between the two aircraft at time  $t_1$ .

The collision avoidance also includes altitude control through deflecting the elevator. Initially, both the host aircraft and intruder move at the same altitude. Once the potential collision is detected, elevator of the host aircraft increases or decreases so that the host aircraft can ascend or descend to avoid the collision. When the collision is avoided, the host aircraft resumes level flight. In this case, the elevation can be considered as pitch, and the control command is

$$\Theta_{cmd} = k_p^\Theta e_3 + k_i^\Theta \int e_3 dt + k_d^\Theta \frac{de_3}{dt} \quad (39)$$

$$e_3 = \begin{cases} h^d - h & t < t_1 \\ h^d + h_c \tan(\underbrace{\arctan \frac{z_a - z_t}{x_a - x_t} + \beta_r^d - \Theta}_{\text{Altitude correction term}}) & t \geq t_1. \end{cases} \quad (40)$$

Here  $h^d$  is the desired altitude,  $h_c$  is a constant used to generate the desired altitude offset and  $\arctan \frac{z_a - z_t}{x_a - x_t} + \beta_r^d$  is the desired elevation during the encounter course.  $k_p^\Theta$ ,  $k_i^\Theta$  and  $k_d^\Theta$  are proportional, integral and derivative gains of the altitude PID controller. The altitude correction term aims to change altitude of the host aircraft to the desired level during the collision avoidance course.

## 5 Simulation Results

### 5.1 Performance of the Relative Range Estimation

In this section, we aim to evaluate the performance of the proposed relative range estimation method based on the measured heading angles  $\theta$  when measurement noise is present. Here, the initial heading is  $\theta_0 = 0$ , and heading of the aircraft increases at an angular speed of  $10 \text{ deg/s}$ . Equation (15) is employed to generate the heading information. A zero-mean Gaussian random noise is added to the heading measurements with normal distribution of  $N(0, 0.02)$ . The initial relative range  $r_0$  is set to be  $600 \text{ m}$ . It is shown in simulations that range estimation accuracy is affected by the number of samples. Estimation accuracy degrades when an excessive large or a small number of samples are chosen. The proper number of samples is obtained when mean square errors between the real and estimated relative range reaches minimum. In the considered application as shown in Fig. 3, the number of samples is chosen to be 127.

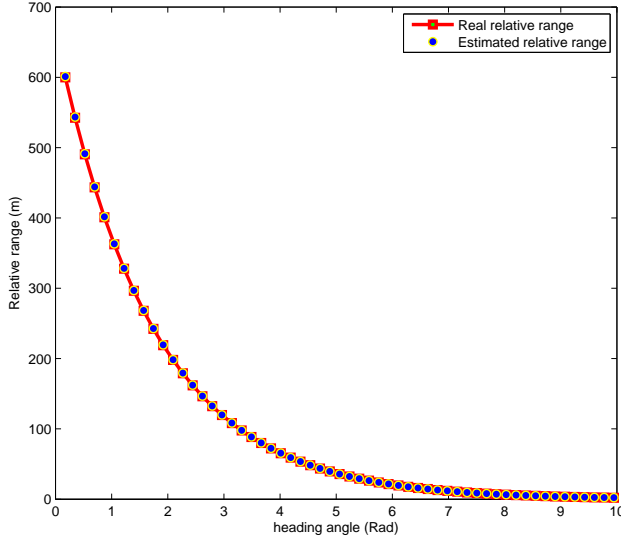


**Fig. 3** Estimation of relative range using the proposed method

The sampled heading with measurement noise is used to construct the matrix  $A$  and vector  $B$  following Eq. (23). Once the solution  $\hat{X}$  is obtained, the estimated relative range  $r_i, i = 1, \dots, N$  can be calculated from Eq. (17) (shown in Fig. 3). The estimated initial relative range  $\hat{r}_0$  is 601.24 m, and the standard deviation for the estimated relative range is 0.38 m. It is observed that the proposed method can estimate the initial relative range with good accuracy.

## 5.2 Collision Avoidance for Typical Collision Scenarios

In this section, we tested performance of the control system for two typical collision scenarios when an intruder follows straight flight: head-on and angle interception. Also, the proposed strategy is applied to an intruder with a curved flight trajectory. Actuator constraints for aileron and elevator are also taken into account. It should be clarified that the proposed collision avoidance strategy can be applied to both manned and unmanned aircraft. Motivated by the availability of the Airborne Systems Laboratory (ASL) [31] as a flight ready testing capability with a reliable fault-tolerant flight control system<sup>1</sup>, we decided to test the collision avoidance strategy using a Cessna model to validate, identify and remedy possible deficiencies before its implementation on UAVs

<sup>1</sup> It is worth noting that the ASL has autonomous capabilities. Collision avoidance algorithms running on an onboard payload can autonomously command the aircraft. Therefore much of its behavior is similar to a UAV.

with safety guarantees. For this purpose we use a high-fidelity Cessna aircraft model from the Airlib [32] simulation toolbox. The Airlib toolbox provides a graphical software environment in consideration of aeronautical constraints for the design and analysis of aircraft dynamics and control systems. Thus, employment of the Cessna 172 model from the Airlib leads to a reliable performance evaluation of the proposed strategy. Aerodynamic parameters of the Cessna, as shown in Table 1, are used in simulations to test performance of the proposed strategy.

For the head-on case, the host aircraft initially follows a level flight with  $45^\circ$  heading. The intruder follows a straight line and moves towards the host aircraft. Both at an altitude of 60 m. Once the potential collision is detected based on the minimum allowable range, the host aircraft starts the collision avoidance strategy by keeping the relative bearing of  $40^\circ$  and relative elevation of  $5^\circ$  during the encounter course. Control gains for heading are chosen to be  $k_p^\psi = 1.5$ ,  $k_i^\psi = 0$  and  $k_d^\psi = 0.05$ . Control gains for pitch are  $k_p^\Theta = -0.01$ ,  $k_i^\Theta = -0.0021$  and  $k_d^\Theta = -0.01$ . Another PID controller is used to implement the BTT control to generate aileron command with control gains  $k_p = -0.05$ ,  $k_i = -0.1$  and  $k_d = 0$ . It is noticed from Fig. 4 that the host aircraft flies sideways on the horizontal plane and increases height to avoid collision. Once collision avoidance is achieved, the host aircraft resumes its pre-arranged route. For the angle interception scenario, the intruder aircraft moves with initial heading of  $135^\circ$  and the host aircraft of  $45^\circ$ . It is seen from Fig. 5 that the collision avoidance has been achieved when the desired relative bearing is  $60^\circ$  and relative elevation is  $-35^\circ$  during the encounter course. The control gains are chosen to be  $k_p = 0.7$  and  $k_i = 12$ . In Fig. 6, the intruder initially moves towards the host aircraft with a constant heading. During the encounter course, the intruder changes heading to follow a curved flight trajectory with varying velocity from 54 m/s to 56 m/s. In this case, potential collision is avoided by keeping a relative bearing of  $30^\circ$  and relative elevation of  $5^\circ$ . Control gains are  $k_p^\psi = 1.7$ ,  $k_i^\psi = 0$ ,  $k_d^\psi = 0.045$  for the heading, and  $k_p^\Theta = -0.02$ ,  $k_i^\Theta = -0.004$ ,  $k_d^\Theta = -0.015$  for the pitch. It is seen that the host aircraft follows a spiral trajectory in the horizontal plane and increases height to avoid the collision during the encounter course.

We investigate how the minimum relative range changes with variations in the desired relative bearing and elevation for the straight flight intruder. Table 2 summarizes the distribution of minimum relative range for different relative bearing and elevation. It is noticed that for a given relative elevation, the minimum relative range increases with an increase in relative bearing. This indicates that when the desired relative bearing is larger, the host aircraft tends to follow a spiral-like trajectory with a larger distance from the intruder. For a given desired relative bearing, the same trend can also be observed. Therefore, increasing relative bearing and elevation can help to avoid spatial collision with safety guarantees.

**Table 1** Parameters of the Cessna 172

| Parameters   | Value             |
|--|-------------------|
| $m$ : Gross mass with full tank  | 1043.3 $kg$       |
| $g$ : Gravitational acceleration   | 9.80665 $ms^{-2}$ |
| $\rho$ : Air density   | 1.201 $kgm^{-3}$  |
| $S$ : Aircraft wing area   | 16.17 $m^2$       |
| $b$ : Wing Span  | 10.91 $m$         |
| $I_{xx}$ : Moment of inertia about $x$ -axis   | 1285.3 $kgm^2$    |
| $I_{yy}$ : Moment of inertia about $y$ -axis   | 1824.9 $kgm^2$    |
| $I_{zz}$ : Moment of inertia about $z$ -axis   | 2666.9 $kgm^2$    |
| $I_{xz}$ : Product of inertia  | 0                 |
| $C_{L0}$ : Aircraft lift curve intercept   | 0.31              |
| $C_L^\alpha$ : Aircraft lift curve slope   | 5.143             |
| $C_L^{\dot{\alpha}}$ : Change in lift coefficient with time rate of angle of attack            | 1.3714            |
| $C_L^{\delta_e}$ : Change in lift coefficient with elevator control                            | 0.43              |
| $C_L^q$ : Change in lift coefficient with pitching   | 3.9               |
| $C_L^M$ : Change in lift coefficient with pitching moment                                      | 0                 |
| $C_{D0}$ : Minimum drag  | 0.031             |
| $e$ : Efficiency factor  | 1                 |
| $\mathcal{AR}$ : Aspect ratio  | 7.32              |
| $C_D^{\delta_e}$ : Elevator drag contribution  | 0.06              |
| $C_D^{\delta_a}$ : Aileron drag contribution   | 0.13              |
| $C_D^M$ : Change in drag coefficient with pitching moment                                      | 0                 |
| $C_Y^\beta$ : change in side force coefficient with sideslip angle                             | -0.31             |
| $C_Y^{\delta_a}$ : Aileron effect on side fore coefficient                                     | 0                 |
| $C_Y^p$ : Change in side force coefficient with rolling rate                                   | -0.037            |
| $C_Y^r$ : Change in side force coefficient with yaw rate                                       | 0.21              |
| $C_l^\beta$ : Change in rolling moment coefficient with sideslip angle                         | -0.089            |
| $C_l^{\delta_a}$ : Change in rolling moment coefficient with aileron deflection                | -0.178            |
| $C_l^p$ : Change in rolling moment coefficient with roll rate                                  | -0.47             |
| $C_l^r$ : Change in rolling moment coefficient with yaw rate                                   | 0.096             |
| $C_{m0}$ : Zero lift pitching moment coefficient   | -0.015            |
| $C_m^\alpha$ : Change in pitching moment coefficient with angle of attack                      | -0.89             |
| $C_m^{\delta_e}$ : Change in pitching moment coefficient with elevator deflection              | -1.28             |
| $C_m^{\dot{\alpha}}$ : Change in pitching moment coefficient with time rate of angle of attack | -4.8438           |
| $C_m^q$ : Change in pitching moment coefficient with pitching rate                             | -12.4             |
| $C_m^M$ : Change in pitching moment coefficient with pitching moment                           | 0                 |
| $C_n^\beta$ : Change in yaw moment coefficient with sideslip angle                             | 0.065             |
| $C_n^{\delta_a}$ : Change in yaw moment coefficient with aileron deflection                    | -0.053            |
| $C_n^p$ : Change in yaw moment coefficient with rolling rate                                   | -0.03             |
| $C_n^r$ : Change in yaw moment coefficient with yaw rate                                       | -0.099            |



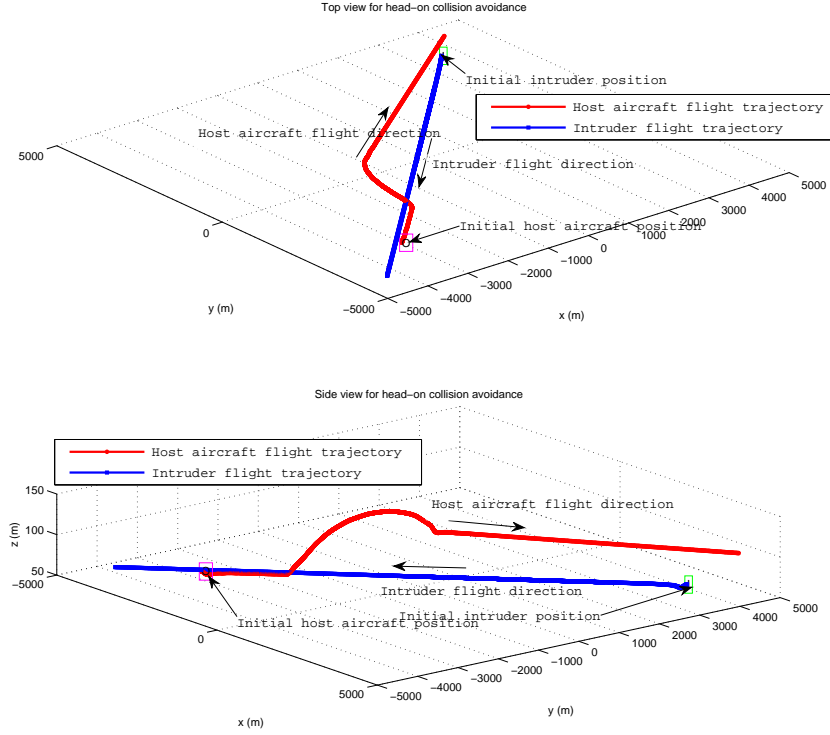


Fig. 4 Collision avoidance for the head-on scenario

## 6 Conclusion and future work

In this paper, a feasible spatial collision avoidance strategy is proposed. The host UAV is controlled to maintain a safe relative range from the intruder by keeping the desired relative bearing and elevation during the collision course. The switching control system is also designed to determine the time moment to trigger the collision avoidance strategy. Performance of the proposed collision avoidance strategy is verified in typical collision scenarios. It is demonstrated that the collision avoidance can be achieved using the proposed strategy. We are currently working towards the implementation of this approach on our ASL platform where the simulated scenarios presented here will be tested using two aircraft. Future work also includes testing the proposed strategy for scenarios when UAVs are with variable velocity.

**Acknowledgements** This research was supported under Australian Research Council's Linkage Projects funding scheme (project number LP100100302) and the Smart Skies Project, which is funded, in part, by the Queensland State Government Smart State Funding Scheme.

本文提出了一种可行的空中避碰策略。在碰撞过程中，通过保持所需的相对方位和仰角，可以控制主无人机与入侵机之间维持一个安全的相对距离。设计了切换控制系统，确定了触发避碰策略的时间矩。在典型的碰撞场景中，验证了该策略的有效性。仿真结果表明，该策略能够有效地避免碰撞。我们目前正致力于在我们的ASL平台上实现这一方法，在这里所展示的模拟场景将使用两架飞机进行测试。未来的工作还包括测试所提出的策略在无人机具有可变速度的情况下。

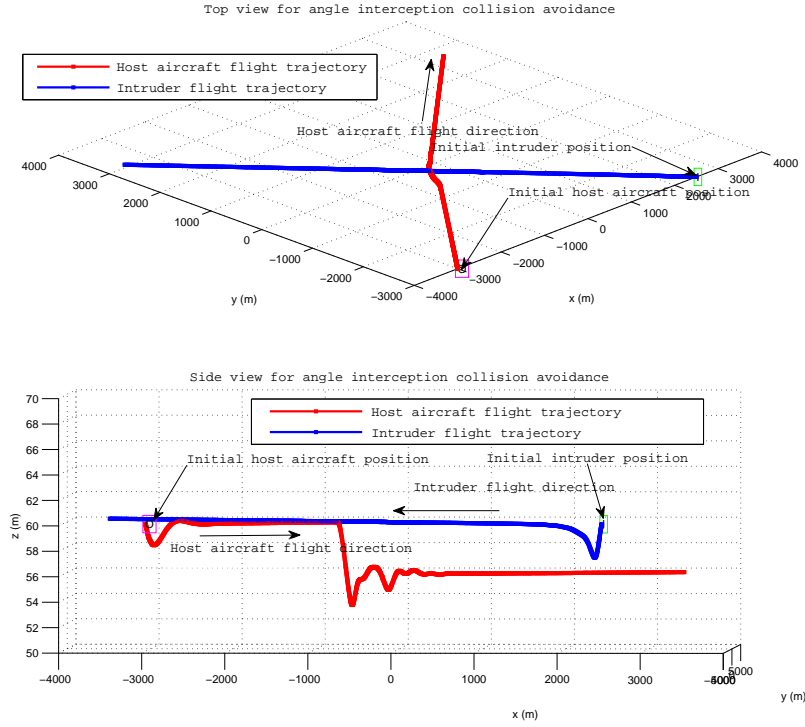
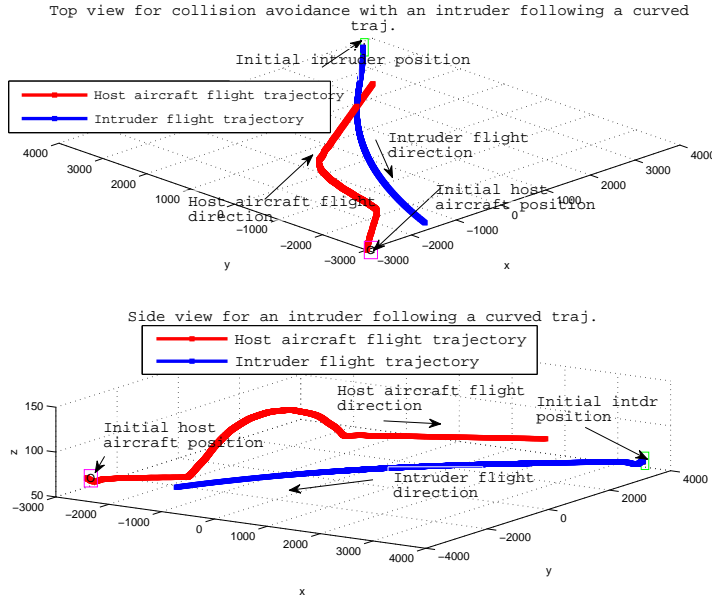


Fig. 5 Collision avoidance for angle interception scenario

## References

1. N. J. S. Stacy, D. W. Craig, J. Staromlynska, and R. Smith, "The global hawk UAV australian deployment: Imaging radar sensor modifications and employment for maritime surveillance," in *IEEE International Geoscience and Remote Sensing Symposium*, vol. 2, 2002, pp. 699 – 701.
2. J. G. Drew, R. Shaver, K. F. Lynch, M. A. Amouzegar, and D. Snyder, *Unmanned aerial vehicle end-to-end support considerations*. RAND Corporation, 2005.
3. J. Downs, R. Prentice, S. Dalzell, A. Besachio, C. M. Ivler, M. B. Tischler, and M. H. Mansur, "Control system development and flight test experience with the MQ-8B fire scout vertical take-off unmanned aerial vehicle (VTUAV)," in *American Helicopter Society 63rd Annual Forum*. Virginia Beach, VA: May, 2007.
4. M. T. DeGarmo, "Issues concerning integration of unmanned aerial vehicles in civil airspace," MITRE, Tech. Rep., 2004.
5. O. of the Secretary of Defense, *Unmanned Systems Roadmap*. Department of Defense, 2007.
6. L. Mejias, J. Ford, and J. Lai, "Towards the implementation of vision-based UAS sense-and-avoid," in *Proceedings of the 27th International Congress of the Aeronautical Sciences (ICAS 2010 CD-Rom)*, 2010.
7. L. Mejias, S. Mcnamara, J. Lai, and J. J. Ford, "Vision-based detection and tracking of aerial targets for uav collision avoidance," in *Proceedings of the 2010 IEEE/RSJ International Conference on Intelligent Robots and Systems (IROS)*, October 2010, pp. 87–92.



**Fig. 6** Collision avoidance for the intruder with a curved flight trajectory

**Table 2** Minimum Relative Range for Head-on Collision Avoidance for the Straight Flight Intruder

| Rel. elevation $\beta_r$ | Rel. bearing $\alpha_r$ |         |         |         |         |
|--------------------------|-------------------------|---------|---------|---------|---------|
|                          | 25°                     | 30°     | 35°     | 40°     | 45°     |
| 5°                       | 1191.07                 | 1304.04 | 1428.60 | 1561.37 | 1698.01 |
| 6°                       | 1240.49                 | 1349.71 | 1470.98 | 1600.49 | 1733.35 |
| 7°                       | 1290.93                 | 1396.08 | 1514.18 | 1640.67 | 1769.69 |
| 8°                       | 1341.19                 | 1443.12 | 1557.83 | 1681.75 | 1806.98 |
| 9°                       | 1404.91                 | 1495.74 | 1602.40 | 1723.47 | 1845.20 |
| 10°                      | 1436.49                 | 1568.98 | 1656.93 | 1765.29 | 1884.40 |
| 11°                      | 1493.47                 | 1574.88 | 1733.81 | 1815.49 | 1924.63 |
| 12°                      | 1523.02                 | 1671.25 | 1743.40 | 1883.16 | 1965.63 |
| 13°                      | 1613.41                 | 1674.78 | 1779.70 | 1891.94 | 2017.95 |
| 14°                      | 1682.81                 | 1750.93 | 1792.57 | 1918.30 | 2034.67 |
| 15°                      | 1725.52                 | 1806.63 | 1843.64 | 2062.97 | 2160.20 |

8. J. Lai, L. Mejias, and J. J. Ford, "Airborne Vision-based Collision-Detection System," *Journal of Field Robotics*, vol. 28, no. 2, pp. 137–157, 2011.
9. J. S. Lai, J. J. Ford, L. Mejias, P. J. O'Shea, and R. A. Walker, "Detection versus false alarm characterisation of a vision-based airborne dim-target collision detection system," in *DICTA 2011 : Digital Image Computing : Techniques and Applications*, Noosa, QLD, December 2011. [Online]. Available: <http://eprints.qut.edu.au/46624/>
10. S. Han, H. Bang, and C. Yoo, "Proportional navigation-based collision avoidance for uavs," *International Journal of Control, Automation, and Systems*, vol. 7, no. 4, pp.

- 553–565, 2009.
11. N. F. T. Tarnopolskaya, “Optimal cooperative collision avoidance strategy for coplanar encounter: Merz’s solution revisited,” *Journal of Optimization Theory and Applications*, vol. 140, pp. 355–375, 2009.
12. G. Roussos and K. J. Kyriakopoulos, “Towards constant velocity navigation and collision avoidance for autonomous nonholonomic aircraft-like vehicles,” in *Joint 48th IEEE Conference on Decision and Control and 28th Chinese Control Conference*, Shanghai, China, Dec. 2009, pp. 5661–5666.
13. D. H. Shim and S. Sastry, “An evasive maneuvering algorithm for uavs in see-and-avoid situations,” in *Proceedings of the American Control Conference*, New York City, USA, Jul. 2007, pp. 3886–3892.
14. M. J. Kochenderfer, J. P. Chryssanthacopoulos, L. P. Kaelbling, and T. Lozano-Perez, “Model-based optimization of airborne collision avoidance logic,” MIT, Lincoln Laboratory, Tech. Rep., 2010.
15. J. Saunders and R. Beard, “Reactive vision based obstacle avoidance with camera field of view constraints,” in *AIAA Guidance, Navigation and Control Conference and Exhibit*, Honolulu, Hawaii, Aug. 2008.
16. S. Shandy and J. Valasek, “Intelligent agent for aircraft collision avoidance,” in *AIAA Guidance, Navigation and Control Conference and Exhibit*, Montreal, Canada, Aug. 2001, pp. AIAA–2001–4055.
17. R. Holdsworth, “Autonomous in-flight plan planning to replace pure collision avoidance for free aircraft using automatic dependent surveillance broadcast,” Ph.D. dissertation, Department of Electrical Engineering at Swinburne University, Nov. 2003.
18. A. Viquerat, L. Blackhall, A. Reid, S. Sukkarieh, and G. Brooker, “Reactive collision avoidance for unmanned aerial vehicle using Doppler radar,” in *6th International Conference on Field and Service Robotics-FSR 2007*, Dec. 2007.
19. H. Voos, “UAV ”see and avoid” with nonlinear filtering and non-cooperative avoidance,” in *Proc. 13th IASTED Int. Conf. Robotics and Applications*, Wurzburg, Germany, 2007.
20. O. Shakernia, W. Z. Chen, and V. M. Raska, “Passive ranging for uav sense and avoid applications,” in *Proc. AIAA Infotech@Aerospace Conf.*, Arlington, Virginia, 2005, pp. 1–10.
21. A. Beyeler, J. C. Zufferey, and D. Floreano, “Vision-based control of near-obstacle flight,” *Autonomous Robots*, vol. 27, no. 3, pp. 201–219, 2009.
22. S. Griffiths, J. Saunders, A. Curtis, B. Barber, T. McLain, and R. Beard, “Obstacle and terrain avoidance for miniature aerial vehicles,” in *Advances in Unmanned Aerial Vehicles*. Springer, 2007, pp. 213–244.
23. P. Angelov, C. D. Bocaniala, C. Xideas, C. Patchett, D. Ansell, M. Everett, and G. Leng, “A passive approach to autonomous collision detection and avoidance in uninhabited aerial systems,” in *Proc. 10th Int. Conf. on Computer Modeling and Sim.*, Cambridge, U.K., 2008, pp. 64–69.
24. M. Shah, A. Hakeem, and A. Basharat, “Detection and tracking of objects from multiple airborne cameras,” *The International Society for Optical Engineering*, 2006.
25. D. J. Lee, R. W. Beard, P. C. Merrell, and P. Zhan, “See and avoidance behaviors for autonomous navigation,” *SPIT optics east, robotics technologies and architecture, mobile robot XVII*, vol. 5609-05, 2004.
26. K. Nordberg, P. Doherty, G. Farneback, P. E.-F. G. Granlund, A. Moe, and J. Wiklund, “vision for a UAV helicopter,” in *Proc. IROS’02 workshop on aerial robotics*, 2002.
27. M. A. Christodoulou and S. G. Kodaxakis, “Automatic commercial aircraft-collision avoidance in free flight: The three-dimensional problem,” *IEEE transactions on intelligent transportation systems*, vol. 7, pp. 242–249, 2006.
28. K. N. Boyadzhiev, “Spirals and conchospirals in the flight of insects,” *The College Mathematics Journal*, vol. 30, no. 1, pp. 23–31, 1999.
29. G. Ambrosino, M. Ariola, U. Ciniglio, F. Corrado, E. D. Lellis, and A. Pironti, “Path generation and tracking in 3-D for UAVs,” *IEEE Transactions on Control Systems Technology*, vol. 17, no. 4, 2009.
30. B. L. Stevens and F. L. Lewis, *Aircraft Control and Simulation*, 2nd ed. John Wiley and Sons, Inc., 2003.

- 
31. D. Greer, R. Mudford, D. Dusha, and R. Walker, "Airborne systems laboratory for automation research," in *27th International Congress of the Aeronautical Sciences*, 2010.
  32. M. Rauw, *FDC 1.2-A SIMULINK Toolbox for Flight Dynamics and Control Analysis*, 2<sup>nd</sup> ed. M. O. Rauw, May 2001.